The metabolic landscape in chronic rotator cuff tear reveals tissue-region-specific signatures

Cyriel Sebastiaan Olie[1] (iD), René van Zeijl[2], Salma el Abdellaoui[1], Arjen Kolk[3], Celeste Overbeek[3], Rob G.H.H. Nelissen[3] (iD), Bram Heijs[2]* (iD) & Vered Raz[1]* (iD)

[1]*Human Genetics Department, Leiden University Medical Center, Leiden, The Netherlands;* [2]*Center for Proteomics and Metabolomics, Leiden University Medical Center, Leiden, The Netherlands;* [3]*Department of Orthopedics, Leiden University Medical Center, Leiden, The Netherlands*

Abstract

Background   Degeneration of shoulder muscle tissues often result in tearing, causing pain, disability and loss of independence. Differential muscle involvement patterns have been reported in tears of shoulder muscles, yet the molecules involved in this pathology are poorly understood. The spatial distribution of biomolecules across the affected tissue can be accurately obtained with matrix-assisted laser desorption/ionization mass spectrometry imaging (MALDI-MSI). The goal of this pilot study was to decipher the metabolic landscape across shoulder muscle tissues and to identify signatures of degenerated muscles in chronic conditions.
Methods   Paired biopsies of two rotator cuff muscles, torn infraspinatus and intact teres minor, together with an intact shoulder muscle, the deltoid, were collected during an open tendon transfer surgery. Five patients, average age 65.2 ± 3.8 years, were selected for spatial metabolic profiling using high-spatial resolution (MALDI-TOF) and high-mass resolution (MALDI-FTICR) MSI in negative or positive ion mode. Metabolic signatures were identified using data-driven analysis. Verifications of spatial localization for selected metabolic signatures were carried out using antibody immunohistology.
Results   Data-driven analysis revealed major metabolic differences between intact and degenerated regions across all muscles. The area of degenerated regions, encompassed of fat, inflammation and fibrosis, significantly increased in both rotator cuff muscles, teres minor (27.9%) and infraspinatus (22.8%), compared with the deltoid (8.7%). The intact regions were characterized by 49 features, among which lipids were recognized. Several of the identified lipids were specifically enriched in certain myofiber types. Degenerated regions were specifically marked by the presence of 37 features. Heme was the most abundant metabolite in degenerated regions, whereas Heme oxygenase-1 (HO-1), which catabolizes heme, was found in intact regions. Higher HO-1 levels correlated with lower heme accumulation.
Conclusions   Degenerated regions are distinguished from intact regions by their metabolome profile. A muscle-specific metabolome profile was not identified. The area of tissue degeneration significantly differs between the three examined muscles. Higher HO-1 levels in intact regions concurred with lower heme levels in degenerated regions. Moreover, HO-1 levels discriminated between dysfunctional and functional rotator cuff muscles. Additionally, the enrichment of specific lipids in certain myofiber types suggests that lipid metabolism differs between myofiber types. The signature metabolites can open options to develop personalized treatments for chronic shoulder muscles degeneration.

Keywords   Rotator cuff tear; MALDI-MSI; Muscle degeneration; Myofiber type

Introduction

Musculoskeletal conditions in adults, which are often chronic, cause pain and lead to reduced function.[1,2] Shoulder pathologies are a prominent cause of musculoskeletal disability during adulthood.[3] The shoulder joint is under repetitive biomechanical stress, and thus, the prevalence of shoulder pathologies greatly increases with age.[4]

The importance of the shoulder is stressed by its impact on mobility and functioning of the entire upper extremity including hands. Shoulder motion is carried out by the four rotator cuff (RC) muscles, which consists of the subscapularis, supraspinatus (SSp), infraspinatus (ISp) and the teres minor (Tmi). Together with the deltoid (Del), the RC muscles ensure stability and mobility of the shoulder joint. The SSp tendon is frequently torn in shoulder pathologies, and in the more severe conditions, the ISp tendon is often also torn.[4-6] Tissue pathology in RC tear is characterized by muscle degeneration, which is marked by atrophy and fat infiltration. The extent of age-associated degeneration differs between the shoulder muscles. Atrophy of the SSp and subscapularis starts at younger ages compared with ISp.[7] In contrast, the Tmi is less affected by age.[7] Muscle histology of ISp with a torn tendon confirmed higher degeneration in ISp compared with Tmi or Del.[7] Despite its high prevalence, the molecular landscape in these RC pathologies is not fully discovered.

Studies into differential metabolism have been able to identify biomarkers for diagnosis, prediction or even targets for therapeutic implications for diverse pathologies.[8,9] Importantly, the metabolic state of a tissue can reflect its function.[10] Tissue metabolomics is often performed on bulk extract, which typically does not enable a direct correlation of the identified metabolites with the tissue histology.[11] Matrix-assisted laser desorption/ionization mass spectrometry imaging (MALDI-MSI) allows one to measure metabolites together with their exact spatial localization.[12,13] This procedure can be particularly powerful in musculoskeletal pathologies where the degenerated is predominantly heterogeneous. MALDI-TOF-MSI is generally a faster technology compared with MALDI-FTICR-MSI, enabling high-spatial resolution analysis of larger (series of) tissues. This fast technology comes at the cost of mass resolution and accuracy; therefore, the MALDI-TOF-MSI was complemented with MALDI-FTICR-MSI, which allows accurate mass measurement and thus a more accurate identity assignment of the features. Performing both procedures in positive and negative ion modes enabled the best discovery potential.[12,13] So far, MALDI-MSI studies in healthy skeletal muscles or conditions leading to degeneration were mainly carried out in rodents.[13-18] Yet the link between metabolomic signatures and muscle function could differ between rodents and humans, as muscle biomechanics differ between these organisms.[19] The aim of this pilot study was to decipher the molecular landscape and to identify molecular signatures to degenerated muscle tissue in chronic conditions by applying spatial metabolomics on human RC muscles.

Methods

Sample collection

Muscle biopsies from two RC muscles, ISp and Tmi, and a shoulder muscle, Del, were collected from five patients with a torn ISp pathology during an open tendon transfer surgery. Details of the surgery are described in Henseler et al.[20] In all patients, the ISp was torn with a retraction grade larger than 3 cm, whereas the Tmi was not torn.[20] All patients suffered from RC functional deficit, and the open tendon transfer surgery aimed to replace the function of the torn muscle. To prevent complication from unnecessary damage during the surgical procedure, the surgical view was kept to a minimum, allowing a biopsy from ISp, Tmi and Del. Hence, the most often damaged SSp could not be biopsied in this procedure. The biopsies were taken from the muscle belly in the surgical view, and histology staining confirmed the presence of myofibers in the tissue. The biopsies were directly frozen in liquid nitrogen and stored at −80°C. Muscle biopsies from five patients at similar age were selected for this study (Supporting Information, *Table* S1). Image collection after magnetic resonance imaging with arthrography (MRA) was carried out as previously described.[7] The study was approved by the Medical Ethical Committee of the Leiden University Medical Center, P11.183, and informed consent was obtained from the patients involved.

Sample preparation

Ten-micrometre thick tissue sections were cut using a cryostat (Leica, Solms, Germany), and sequential sections were thaw-mounted on four indium–tin-oxide (ITO)-coated glass slide (Bruker Daltonics, Bremen, Germany) and stored at −80°C. In addition, sequential sections for immunofluorescence staining were mounted on Superfrost plus glass slides (Menzel-Gläser, Braunschweig, Germany) and stored at −20°C. The ITO slides were freeze-dried before applying either N-(1-naphthyl)ethylenediamine dihydrochloride [7 mg/mL in solvent A (80% ACN, 10% methanol and 10% MilliQ)] on two ITO slides as MALDI matrix for negative ion mode analyses, or *nor*-harmane (7 mg/mL in solvent A) on the remaining two slides, as MALDI matrix for positive ion mode analyses. Both matrices were applied homogeneously using a SunCollect sprayer (SunChrom, Friedrichsdorf, Germany) with the following settings used for both matrices: gas pressure 35 psi, 13 layers in total (three at

10 µL/min, followed by three layers at 30 µL/min and finished by four layers at 40 µL/min) were applied at a distance of 20 mm (Z) and a line distance of 1 mm and speed(x)(y) = med(1).

Mass spectrometry imaging

MALDI-MSI at 20 × 20 µm^2 pixel size was performed in both negative and positive ion modes using a rapifleX MALDI-TOF/TOF mass spectrometer (Bruker Daltonics, Bremen, Germany). Negative ion mode was analysed with the mass range of 100–1000 mass-to-charge ratio (*m/z*), and a total of 1000 shots per pixel were acquired at 10 kHz laser repetition rate.

Data for positive ion mode were acquired with the following settings: mass range 70–1500 *m/z*, 50 shots per pixel at 5 kHz laser repetition. Data acquisition was performed using the fleX-software suite (Bruker Daltonics). High resolving power MALDI-FTICR-MSI was performed at 70 × 70 µm^2 pixel size in both positive and negative ion mode using a 12 T SolariX XR mass spectrometer (Bruker Daltonics). For negative ion mode, the recorded mass range was 100–1000 *m/z*, and a total of 500 laser shots were recorded per pixel. For positive ion mode: 70–1500 *m/z*, and a total of 30 laser shots per pixel. Data acquisition was performed using ftmsControl and flexImaging v5.0 software packages (Bruker Daltonics).

Following MALDI-MSI analysis, excess MALDI matrix was removed using 70% ethanol (washed for 5 min two times). The tissue sections were then stained using the Gomori-trichrome staining.[21] In brief, the slides were submerged in haematoxylin for 5 min after which the slide were washed in running water and subsequently stained with trichrome for 10 min. The slides were then briefly washed and dehydrated followed by imaging using a digital IntelliSite Ultra-Fast Scanner (Philips, Eindhoven, The Netherlands). Trichrome-stained images were co-registered with MSI data, and regions of interest (ROIs) of intact muscle fibres or degenerated muscle areas were annotated in flexImaging.

Matrix-assisted laser desorption analyses

MALDI-TOF-MSI data were imported into SCiLS lab 2016b (Version 4.01.8781, SCiLS Lab/Bruker Daltonics). The overall average spectrum of the data set was used for feature selection in mMass (Version 5.5.0). Peak picking was performed using the following settings: Baseline correction; precision 15 and relative offset 25, Smoothing; method Savitzky–Golay with window size 0.1 and two cycles followed by peak picking using a signal-to-noise ratio greater than nine (S/N > 9) with picking height at

78. A list of 312 (negative ion mode) and 203 (positive ion mode) *m/z* features was imported back into SCiLS Lab and used for the subsequent analyses. All spectra were root mean square normalized.[22] Discriminative features between different muscles or different ROIs were found using the receiver operating characteristic (ROC) analysis. The ROC analysis was performed on an equal number of random subsets (a third of the total spectra) of spectra to prevent introducing bias towards the larger sized muscles or ROIs (*Table* S2).[23] To prevent under-sampling, the ROC analysis was performed five times, and only features that had an area under the curve (AUC) of ≥ 0.85 or ≤ 0.15 for at least 80% of tests were considered ($0.15 \geq$ AUC ≥ 0.85, ROC presence score $\geq 80\%$). A more accurate *m/z* of the discriminative features was then acquired using the MALDI-FTICR-MSI data, which was analysed separately from the MALDI-TOF. The data of both the MALDI-TOF and MALDI-FTICR systems were calibrated to the same external calibration standard (red phosphorus). The total distributions were also taken into account for matching the FTICR spectra to the TOF. Subsequently, the FTICR peaks within the peak width of the TOF-peaks were considered common/shared. Features that were not found in the MALDI-FTICR data were not included for identity assignment, which was done based on mass matching against the human metabolome database 4.0.[24] The identification search was performed for negative ion mode, using $M - H^-$ as adduct type and a molecular weight tolerance of ±0.01 Da. For the positive ion mode, the following adduct types were included $M + H^+$, $M + Na^+$ and $M + K^+$ with a ±0.05 Da of mass tolerance. Spatial segmentation was performed on the complete list of 312 features (MALDI-MSI TOF, negative ion mode), using the bisecting *K*-means method with the following parameters: Metric: correlation distance, Denoising: weak, and a minimal interval width of ±0.1 Da. Correlation matrices of the region-specific features were created using a hierarchical clustering analysis.

Immunofluorescence

Immunohistochemistry was carried out on sequential sections. Slides were air-dried for 30 min, followed by 30 min blocking using 5% milk in PBST. Subsequently, primary and secondary antibodies were incubated as detailed in *Table* S3. All sections were then mounted with Aqua Polymount. Imaging of the entire muscle was carried out with the Arrayscan VTI HCA, Cellomics (Thermo Fisher Scientific), and image stitching was carried out with the HCA software V6.6.1. Imaging of selected regions was carried out with the Leica DM5500 using the Leica LAS X software v.3.7.2.22383.

Results

Spatial metabolomics offers important insights in the molecular landscape of tissues. In this study, robust mass spectrometry imaging was used to elucidate the spatial metabolome in RC muscles with a torn ISp pathology. The patients included in this study had all torn ISp, intact Tmi and were in their 60s (mean 65.2 ± 3.8 years old), without a gender preference (*Table* S1). Because age is a covariant in RC pathology, we selected patients with a similar age range,[4] minimizing the possibility of finding age-associated changes. The Del, an unaffected shoulder muscle, was accessible in the surgical field and a biopsy was taken for a comparison. Muscle degeneration was assessed from MRA images using the Goutallier score, estimating fat accumulation. Consistent with previous studies,[7,25] in all patients both the Goutallier score, and lipid droplet accumulation were higher in ISp compared with Tmi and Del (*Figures* 1A and S1A).

After confirming tissue quality using histological staining, cross-sections were subjected to MALDI-MSI analyses and subsequently stained to link the metabolic landscape with the tissue histopathology (*Figures* 1B and S1B). Next, a protocol with two MALDI-MSI procedures was set up to find metabolites that were associated with muscle involvement in RC tear pathology. Both MALDI-TOF-MSI and MALDI-FTICR-MSI procedures were carried out in positive and negative ion mode, enabling the best discovery potential. Only features that passed the cut-off criteria of S/N > 9 were considered. In total, 312 or 203 features for negative or positive ion mode respectively were included (*Table* S4).

Potential molecular differences between the three muscles were assessed using a supervised analysis (schematically displayed in *Figure* 2A, i). The average spectra showed similar intensities across the three muscle groups (*Figure* S2A and S2B), and a muscle-specific molecular enrichment or depletion was not found between muscles (*Figure* 2B–2C). This suggests that the metabolic profile is predominantly similar between Del, Tmi and ISp. Subsequently, an unsupervised, data-driven, analysis was applied to find regions with molecular similarities (schematically displayed in *Figure* 2A, ii). The spatial segmentation revealed three prominent clusters that dispersed across all samples (*Figure* 2D and *Table* S2). The average spectra of Clusters 1 and 2 showed opposite peak intensities (*Figure* 2E). In contrast to Clusters 1 and 2, the third cluster contained mainly features with lower masses, among which masses that corresponded to the MALDI matrix (*Figure* 2D). Therefore, Cluster 3 was not considered for further analyses. Strikingly, the clusters' relative area significantly differed between muscle groups (*Figure* 2F). The relative average area of Cluster 1 was higher in Del compared with ISp or Tmi (91.3% vs. 72.1% or 77.2%, respectively; *Figure* 2F). In contrast, the average area of Cluster 2 was proportionally larger in Tmi (27.9%) or ISp (22.8%) compared with Del (8.7%) (*Figure* 2F). The spatial localization of Cluster 1 overlapped with regions showing intact myofibers, whereas Cluster 2 overlapped with regions showing fibrosis and fat, representing degenerated tissue (*Figure* S1B). Comparison of the average spectra of intact and degenerated tissue showed clear differences in abundances of various features (*Figures* 3A, S2C and S2D). Discriminative analysis for the negative ion mode resulted in 14 and 28 features that were specific to intact or degenerated regions, respectively (*Figure* 3B). In positive ion mode, 35 and 9 features were found for intact or degenerated regions (*Figure* 3C). To identify subgroups of spatially correlated molecular features, a Pearson correlation between spatial distribution of the region-specific features was assessed. The correlation matrices showed that within the two previously defined clusters, subclusters were present (*Figure* 3D–3E). Those subcluster represented specific areas in the muscles (*Figure* 3F). Features that were not localized to annotated regions were excluded.

MALDI-FTICR-MSI was then used to accurately assess the masses of the region-specific features. Most features were detected with both mass spectrometers (*Figure* S4A), and their spatial localization was comparable with the MALDI-MSI-TOF (*Figure* S4B and S4C). The accurate mass of the region-specific features was then assigned to metabolites (*Table* S5). Intact myofibers were enriched by a variety of lipids and robustly expressed ATP (506.01 *m/z*) and ADP (426.03 *m/z*) among other metabolites (*Table* S5). In contrast, heme and hemin were the most abundant metabolites that were exclusively found in degenerated regions (*Table* S5).

Heme is mainly catabolized by Heme oxygenase-1 (HO-1), and the expression of HO-1 has been suggested to play a role in tissue degeneration.[26] Therefore, a link between the spatial localization of HO-1 and heme was assessed in degenerated RC muscles. Contrary to heme, HO-1 signal was found within intact regions (*Figure* 4A and 4B). In the severely affected ISp muscles, HO-1 signal was higher compared with the less affected muscles, Del or Tmi (*Figure* 4C). In contrast, heme average levels were lower in ISp compared with Del or Tmi (*Figure* 4D). A significant negative correlation ($r = -0.52$) was found between HO-1 signal and heme accumulation (*Figure* 4E).

Intact regions are marked by the presence of myofibers, which can be recognized by the expression of myosin heavy chain isoforms (MyHC)-2X, 2A and type-1.[27] To assess whether myofiber types were enriched with specific metabolites, a supervised approach was employed (*Figure* 5A). Myofibers positive or negative for MyHC-2A were assigned by eye (*Figure* 5B). With the negative ion mode, 30 features were found as specifically associated with type-2A-positive or type-2A-negative regions (*Figure* 5C and *Table* S6). The positive ion mode analysis resulted in 36 features, of which all were enriched in type-2A-negative regions (*Figure* 5D and *Table* S6). The identified lipids had a
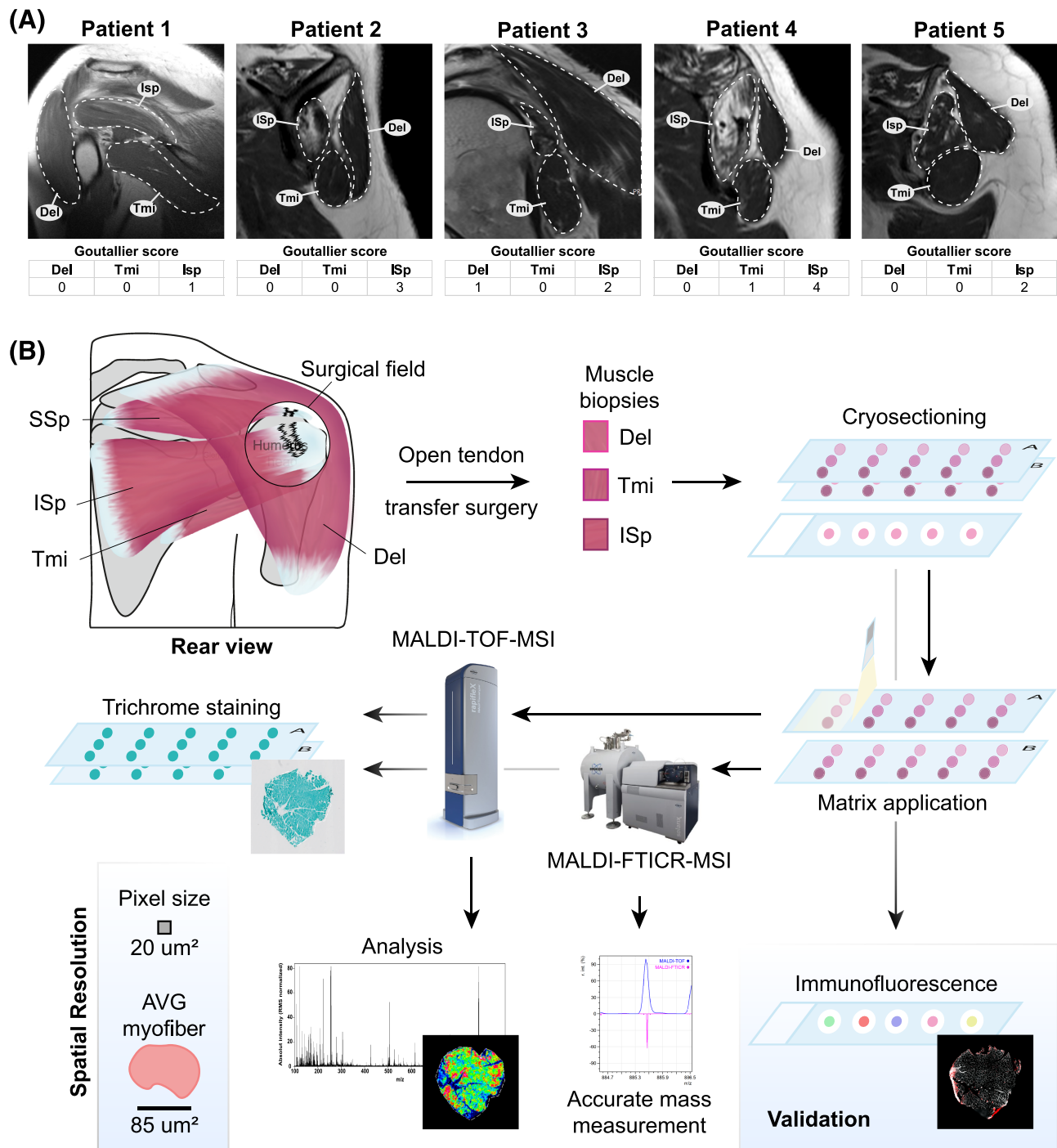
Figure 1 Schematic overview of the study workflow. (*A*). Images of magnetic resonance imaging with arthrography of the shoulder muscles from the same patients whose muscle biopsies were used for MSI. The Del, Tmi and ISp regions are encircled with a dashed line. Goutallier score estimates fat accumulation in the respective muscles. (*B*). A rear schematic view of the diseased shoulder. Encircled is the surgical field with torn tendons that are located under the Del. Biopsies were taken from Del, Tmi and ISp close to the torn location during an open rotator cuff tendon transfer surgery. Sequential cryosections were scanned and analysed by both high-spatial resolution (MALDI-TOF) and high-mass resolution (MALDI-FTICR) MSI in negative and positive ion mode and subsequently were Gomori-trichrome stained. Validation studies of MSI analyses were carried out on sequential sections.

strong spatial association with MyHC-2A-positive or MyHC-2A-negative myofibers (*Figure* 5E). Therefore, the different groups of lipids were analysed. MyHC-2A-negative myofibers had only four features identified to different lipids compared with 16 features in MyHC-2A-positive regions (*Table* S7).
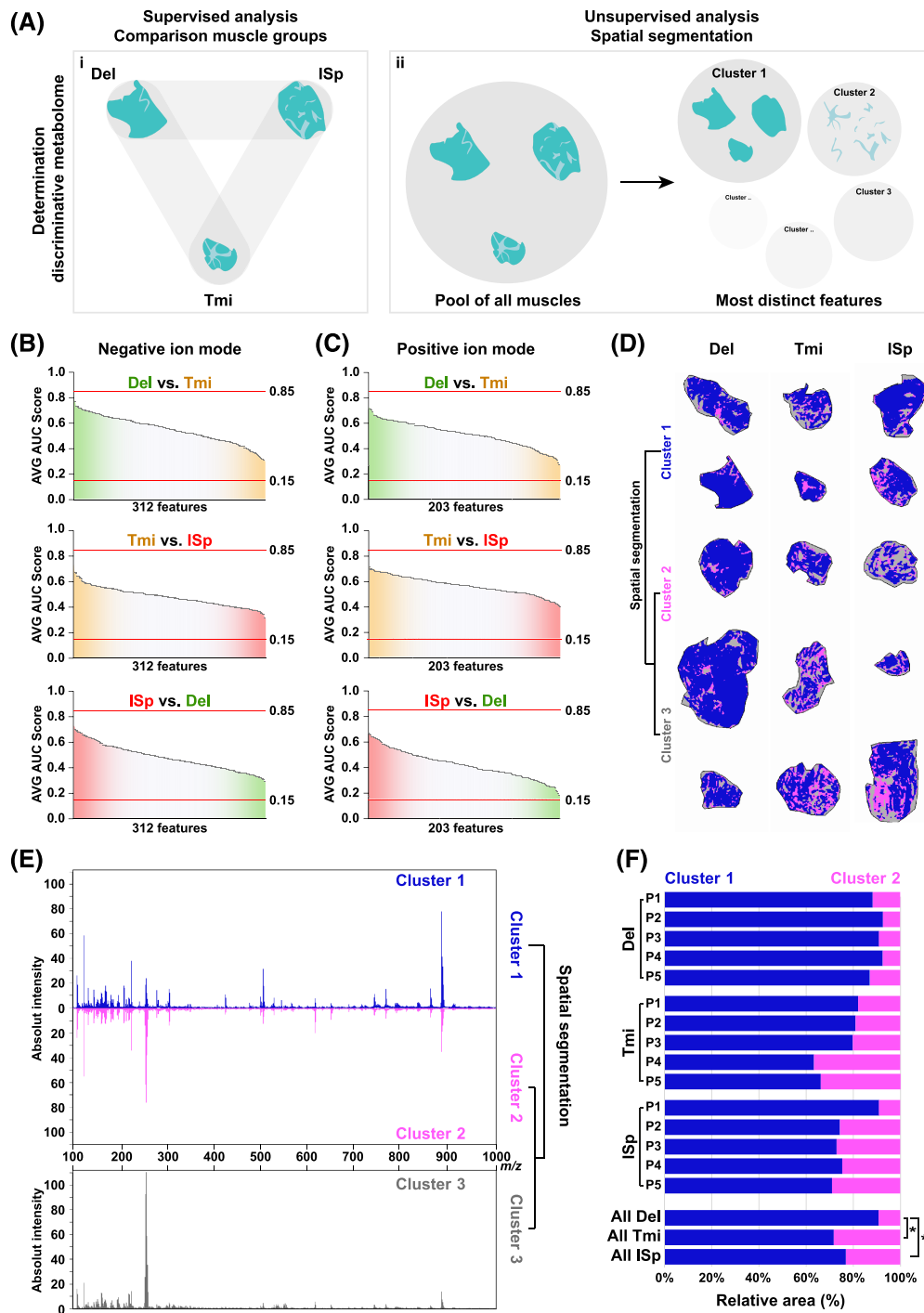
Figure 2 Spatial segmentation shows prominent differences between three clusters but not between muscles. (*A)* Cartoon shows the two different approaches for finding discriminative metabolites. (i) Supervised comparison assessed differences between muscle groups; results are presented in panels (*B*)–(*C*). (ii) Unsupervised analysis using spatial segmentation. The corresponding results are presented in panels (*D*)–(*F*). (*B–C*) An ROC analysis comparing every two-muscle combination (Del vs. Tmi, Tmi vs. ISp and ISp vs. Del) for negative and positive ion modes (panels *C* and *D* respectively). Graphs show the average AUC (*n* = 5) score with standard deviation for all used features. Average AUC score cut-offs at 0.15 and 0.85 are depicted with a red line. Analysis was performed on 312 or 212 features (S/N > 9) for negative or positive ion mode, respectively. (*D*) A spatial representation of the spatial segmentation in all Del, Tmi and ISp muscles (*n* = 15). Intact regions are depicted in blue, degenerated regions in pink and MALDI matrix in grey. (*E)* RMS-normalized average MALDI-TOF-MSI spectra plots specific to the blue (intact region), pink (degenerated region) or grey (MALDI matrix) clusters, as depicted in panel (*D*). (*F*). Bar chart shows the relative area of Clusters 1 and 2, per muscle per patient. The lower bar chart shows the average proportions of the two clusters per muscle. A pair *t*-test was used to assess the significance (*P* < 0.05 = *) between area between muscles. AUC, under the curve.
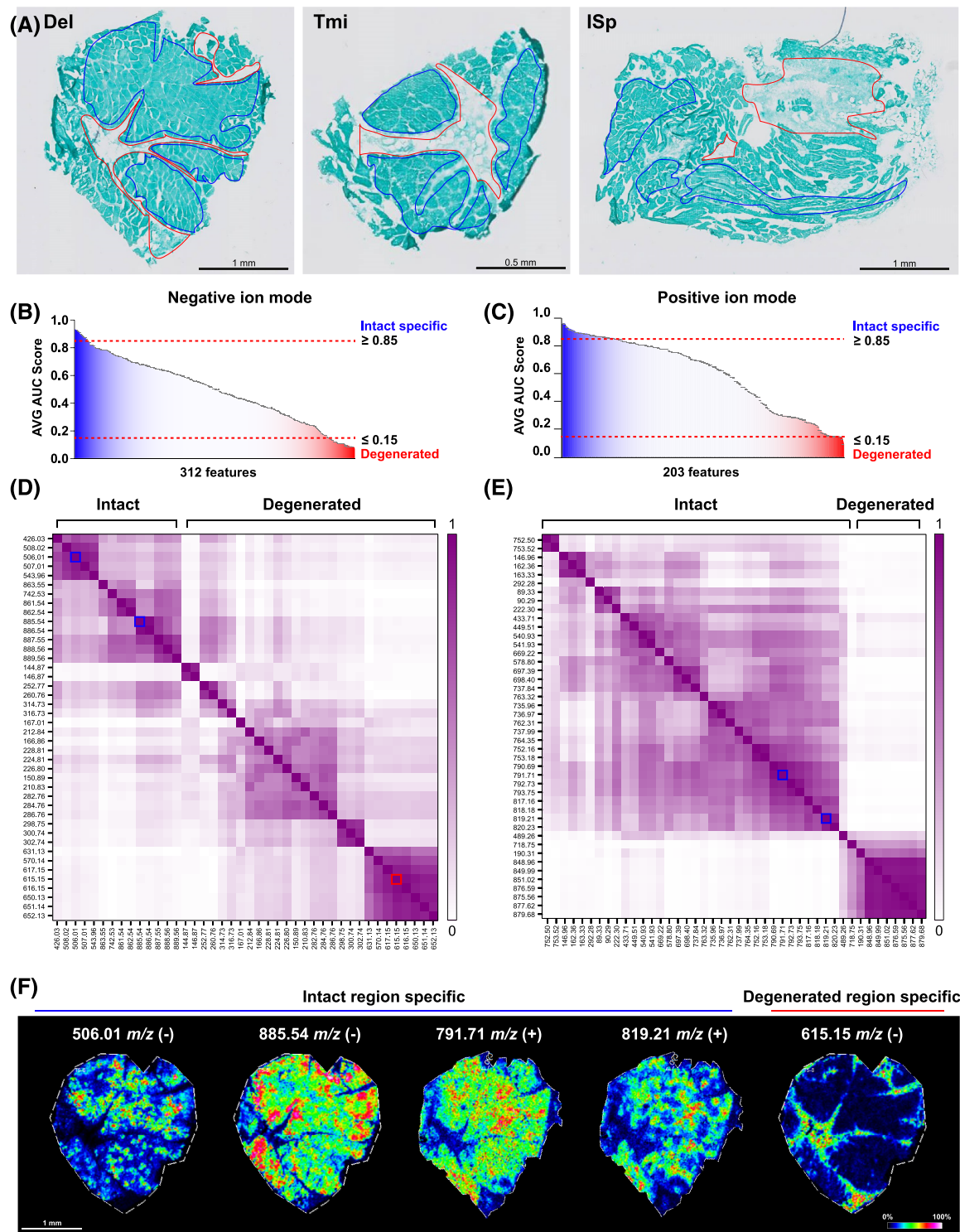
Figure 3 The mass spectra differ between intact and degenerated regions. (*A*) Manual annotation of intact (blue) or degenerated (red) regions in trichrome-stained samples are shown for representative Del, Tmi and ISp. (*B–C*) ROC analysis for the intact muscle regions vs. degenerated muscle regions comparison for negative (*B*) and positive ion (*C*) mode MALDI-MSI. AVG AUC scores of ≥0.85 are considered to be intact muscle-specific features (presented in dark blue) and AVG AUC score ≤ 0.15 are degenerated muscle-specific features (presented in dark red). (*D–E*) Heatmaps of Pearson correlation matrix of the region-specific features between intact and degenerated regions. Panel (*D*) is negative mode (*n* = 42); panel (*E*) is positive mode (*n* = 48). Five features are highlighted as examples with blue (intact) or red (degenerated) lines. (*F*) Images show spatial distribution of four intact (indicated with blue line) and one degenerated (red line) enriched features in a representative muscle. AUC, under the curve.
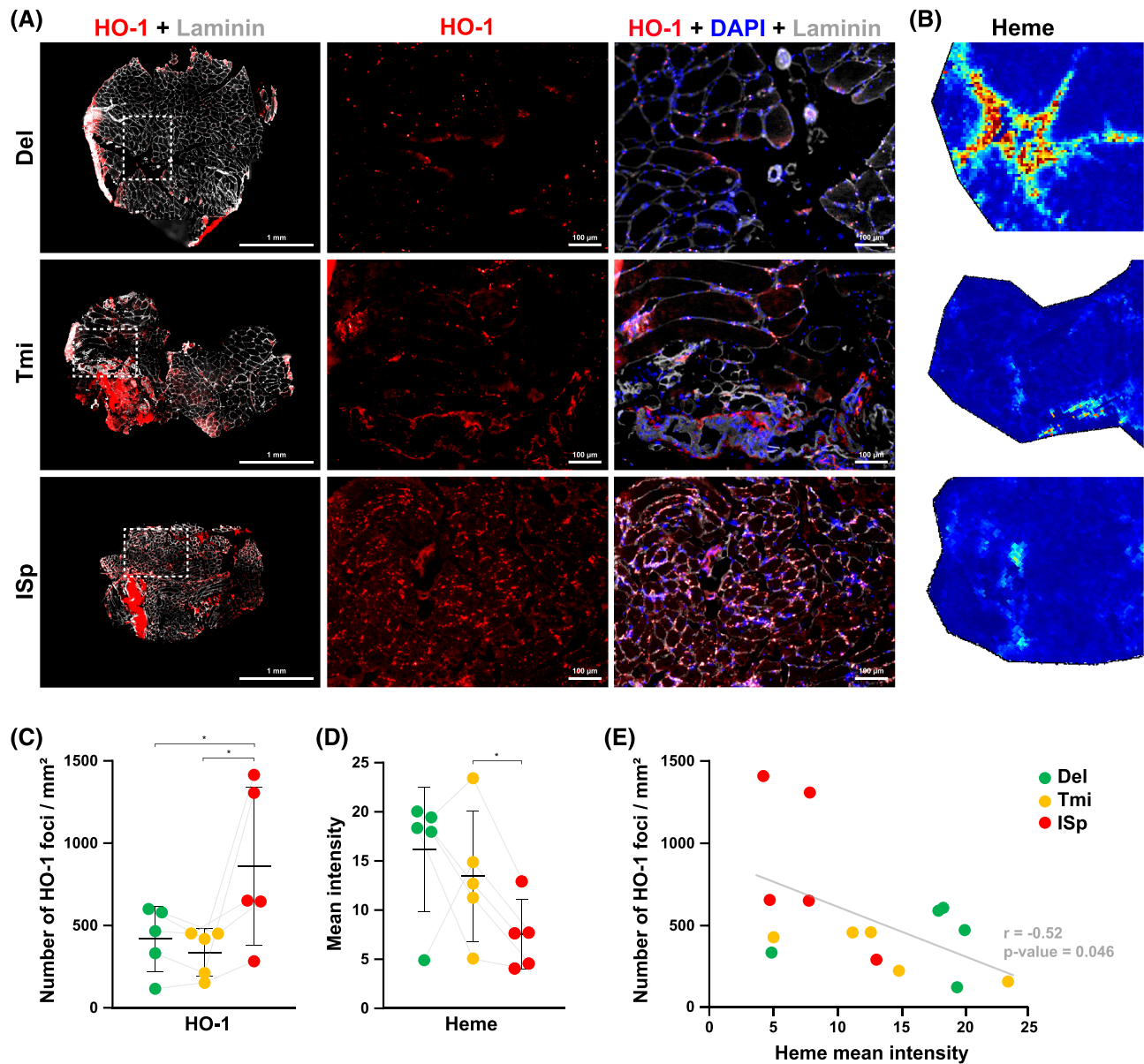
Figure 4 Heme accumulation does not complement with Heme oxygenase-1 localization. (*A*). Representative images show Heme oxygenase 1 (HO-1, red) and laminin (grey) in Del, Tmi and ISp. Scale bar is 1 mm. A magnification of the white dashed squares is shown for HO-1 alone (middle column) or an overlay of HO-1, laminin and a nuclear counterstaining in blue (Dapi) (right column). Scale bar is 100 μm. (*B*) Images show heme distribution in the respective dashed square region. (*C*) Dot plot shows the number of HO-1 foci per area of the muscle. (*D*) Dot plot shows mean intensity of heme in the heme positive regions. (*E*). Scatter plot shows number of HO-1 foci/mm^2 vs. the heme mean intensity. A linear regression is indicated with the grey line. Significance was assessed using the Pearson correlation. For panels (*C*)–(*E*), Del = green, Tmi = yellow and ISp = red. For panels (*C*) and (*D*); transparent lines indicate paired muscles. Significance, indicated with *, was assessed with a paired ratio *t*-test.

Discussion

This pilot study shows the first effort to elucidate the spatial metabolic landscape across different human skeletal muscles. Previous clinical studies showed that ISp is more affected by RC tear compared with Tmi and the adjacent Del muscle.[7] On the basis of those observations, we investigated whether metabolites or lipids could discriminate between the torn and intact muscles. In this study, metabolites or lipids that could discriminate between shoulder muscles were not found. Instead, this study showed that the spatial occupation of compounds specific to intact or degenerated regions differed between muscles. In agreement with MRA analysis of RC pathologies showing that the ISp is more affected compared with Del,[7] metabolic spatial clustering showed higher proportions of intact regions in Del compared with ISp. MRA analysis
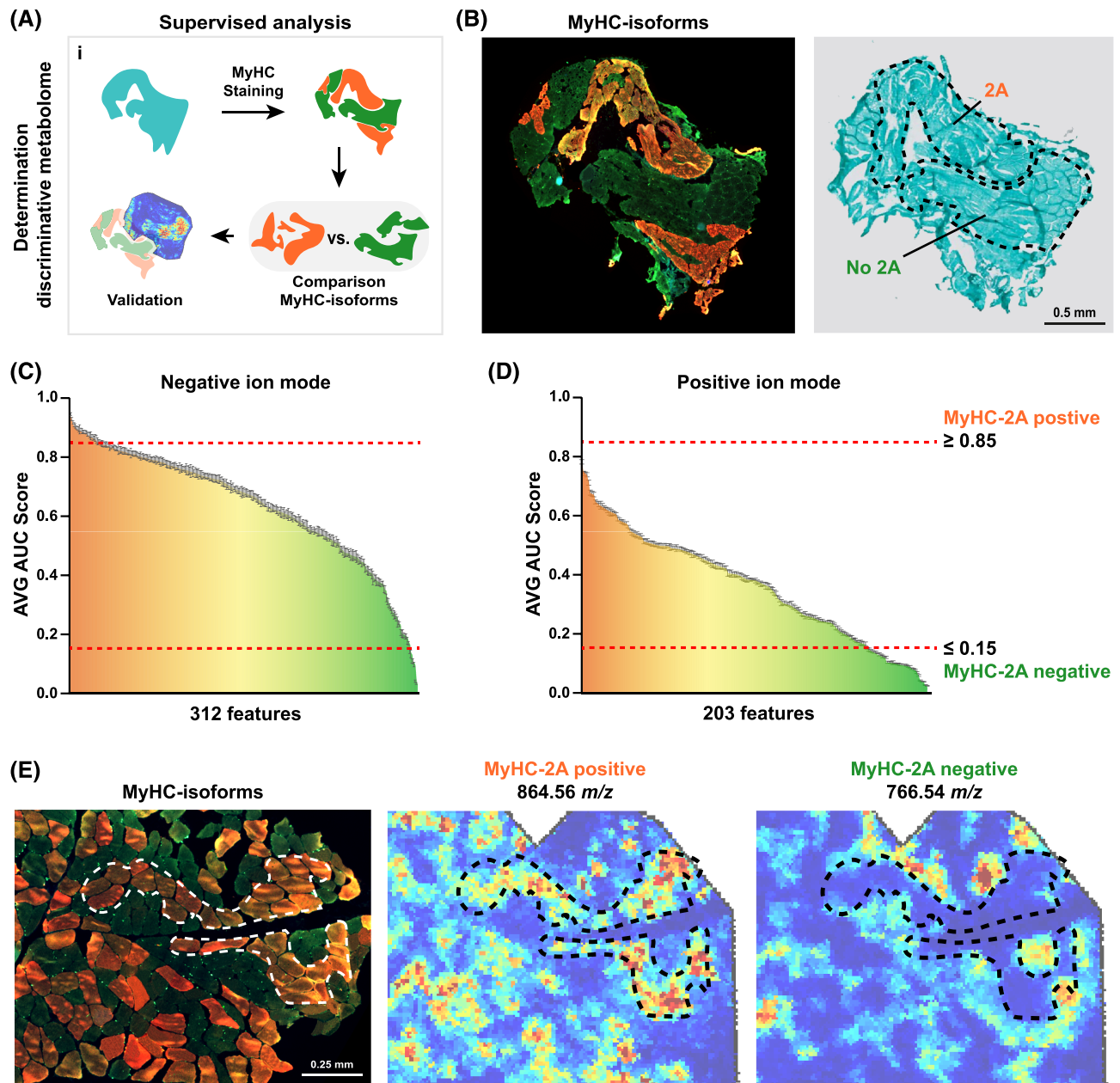
Figure 5 Spatial distribution of myofiber-isotype-specific features. (*A*) Cartoon presents the applied workflow. Tissue sections were first stained for MyHC-isoforms, which was sequentially used to annotate the different MyHC-isoforms. Next, a comparison between the MyHC-2A-positive and MyHC-2A-negative myofibers was performed to identify MyHC-isoform-specific features, which was followed by validation. (*B*) An example of myofiber type regions and the corresponding Trichome staining (right panel). MyHC-2A-positive or MyHC-2A-negative regions are gated with dashed lines. Scale bar is 0.5 mm. (*C*)–(*D*). ROC analysis for the comparison of MyHC-2A-positive vs. MyHC-2A-negative myofibers for negative and positive ion mode, panels (*C*) and (*D*), respectively. Features with AVG AUC score of ≥0.85 are considered to be MyHC-2A specific (presented in dark orange) and AVG AUC score ≤ 0.15 are specific to other MyHC-isotypes (presented in dark green). Features that are coloured yellow could be hybrid specific. (*E*) Immunofluorescence image shows a merged image of MyHC type-1 in blue, type-2X in green and type-2A in red. Spatial distributions of 864.56 and 766.54 *m/z* show a MyHC-2A-independent or MyHC-2A-dependent expression in an example muscle. Dashed lines indicate MyHC-2A-positive regions.

showed only limited fat infiltration in Tmi compared with ISp (*Figure* 1A),[7] but in the muscle biopsies from both muscles, the degenerated regions were equally abundant. In contrast to the MRA, where the entire muscles phenotype is assessed, the biopsies are local, and all were taken from the same surgical view. Thus, the biopsies may not necessarily represent the entire muscle. This is a known limitation in histological approaches.

Despite the unchanged metabolome between dysfunctional ISp and functional Tmi, HO-1 levels were high in the ISp and lower in the Tmi. HO-1 signal was higher in intact regions and was lower in degenerated regions. In non-muscle wounded and degenerated tissues, HO-1 plays a role in cellular protection against oxidative stress.[28-30] Enhanced oxidative capacity is beneficial for skeletal muscle function and protects against pathologies, such as aging and myopathies.[31] The accumulation of HO-1 in the dysfunctional ISp could suggest cellular protection against oxidative stress in the torn muscle. In agreement, muscle disuse in mice leads to elevated HO-1 expression.[32] Also in cardiac dysfunction conditions, HO-1 levels increased and upon mechanical support for cardiac cells HO-1 levels reduced again.[33] It is possible that oxidative stress accumulates in dysfunctional muscle, but not in functional muscle. In addition, a striking negative correlation between heme and HO-1 levels was found across all 15 samples. Heme is highly associated with inflammation, and higher inflammation was reported in mice lacking HO-1.[34-36] This suggests that heme localization was counteracted by an increased HO-1 presence. Yet it remains for future studies to unravel the mechanism regulating HO-1 accumulation in ISp and the potential benefits for tissue regeneration. A potential approach could be to compare disused or damaged muscles in presence or absence in HO-1 with used or again healed muscles. The ratio of heme and HO-1 levels could potentially be a marker for muscle degeneration.

Muscle degeneration is often associated with a disturbance in lipid metabolism.[37-40] Our study showed that intact myofibers were highly enriched in lipids, of which, various lipids were specifically enriched in MyHC-2A-negative myofibers. Different forms of PC lipids detected with MALDI-MSI were reported to be MyHC-isoform specific.[15,41] The limitation of the MALDI-MSI the ability to identify the exact lipid conformation.[42] To elucidate the exact role of lipids in myofibers, one should use other techniques that are more suitable for determining the tissue lipidome.[43] In addition, a technical limitation that could also play a role in detecting muscle-specific molecules is the molecular depth obtained with MALDI-MSI. Other techniques, such as laser capture microdissection mass spectrometry, can reach higher molecular depths but often lack the spatial resolution to assess myofiber-specific enrichment.[44]

In summary, this pilot study presents a high-resolution spatial metabolome in shoulder muscles that successful discrimination between intact and degenerated tissue. A limitation of this study is the low number of included patients. It is possible that muscle-specific molecules could be found with a higher number of patients. The study design allowed statistical paired analysis that overcomes potential inter-patient variability. Muscle degeneration in the shoulder muscles is age associated, and to minimize variations between patients, we performed this pilot study on a small age group (average 65 years old). The observations reported here are related to this age (middle-aged adults) and not for younger or older patients. Most significant, the area of degenerated regions increased in the more severely affected muscle compared with the adjacent Del muscle. We suggest that specific lipids can discriminate between myofiber types. Further research is therefore needed to illuminate the role of the MyHC-isoform associated lipids. Finally, heme characterized the degenerated regions, which in the severely affected muscles was counteracted by increased HO-1 presence.

Acknowledgements

Online supplementary material

Additional supporting information may be found online in the Supporting Information section at the end of the article.

Figure S1. Histological staining indicates infraspinatus as most affected. A. Lipid droplet staining is depicted in red and nuclei are counterstained with DAPI. An overlay with bright-light differential interference contrast (DIC) shows the muscle histology. B. Gomori-Trichrome staining of Del, Tmi and ISp muscles from five patients. Scale bar is 1 mm.

Figure S2. Mass spectra of Del, Tmi and ISp muscles. A-B. RMS-normalized average MALDI-TOF-MSI spectra specific to Del, Tmi and ISp. C-D. RMS-normalized average MALDI-TOF-MSI spectra specific to intact and degenerated regions. Panels A and C are obtained using negative ion mode and panels B and D are of the positive ion mode.

Figure S3. MALDI-FTICR mass spectrometry validates the MALDI-TOF mass spectrometry. A. Comparison of the MALDI-TOF (depicted in black) and MALDI-FTICR (depicted in purple) spectra for negative and positive ion mode. B. Two representative m/z features are depicted as examples. The spectra show smaller peaks indicating higher mass accuracy. The MSI images show a similar spatial distribution between the two mass spectrometers. MALD-FTICR MSI images were recorded with a pixel size of 70x70 μm^2 and MALDI-TOF MSI with 20x20 μm^2. C. Spatial distributions of Heme and PGP(38:0) presented for all muscles ($n = 15$) in MALDI-TOF (annotated in black) and MALDI-FTICR (annotated in purple).

Table S1. Patient information.

Table S2. Number of spectra detected across different muscles.

Table S3. Antibodies used for immunofluorescence.

Table S4. Intensities all 312 and 203 features detected with negative and positive ion mode, respectively (S/N > 0.9).

Table S5. Region-specific features detected with negative and positive ion mode.

Table S6. MyHC-isoform specific features detected with negative and positive ion mode.

Table S7. MyHC-isoform specific lipids.

Conflict of interest

All authors declare no conflict of interest.

References

1. Tieland M, Trouwborst I, Clark BC. Skeletal muscle performance and ageing. *J Cachexia Sarcopenia Muscle* 2018;**9**:3–19.

2. Picavet HS, Schouten JS. Musculoskeletal pain in the Netherlands: prevalences, consequences and risk groups, the DMC(3)-study. *Pain* 2003;**102**:167–178.

3. Greving K, Dorrestijn O, Winters JC, Groenhof F, Van der Meer K, Stevens M, et al. Incidence, prevalence, and consultation rates of shoulder complaints in general practice. *Scand J Rheumatol* 2012;**41**:150–155.

4. Sambandam SN, Khanna V, Gul A, Mounasamy V. Rotator cuff tears: an evidence based approach. *World J Orthop* 2015;**6**:902–918.

5. Huegel J, Williams AA, Soslowsky LJ. Rotator cuff biology and biomechanics: a review of normal and pathological conditions. *Curr Rheumatol Rep* 2015;**17**:476.

6. Craik JD, Mallina R, Ramasamy V, Little NJ. Human evolution and tears of the rotator cuff. *Int Orthop* 2014;**38**:547–552.

7. Raz Y, Henseler JF, Kolk A, Riaz M, van der Zwaal P, Nagels J, et al. Patterns of age-associated degeneration differ in shoulder muscles. *Front Aging Neurosci* 2015;**7**:236.

8. Rinschen MM, Ivanisevic J, Giera M, Siuzdak G. Identification of bioactive metabolites using activity metabolomics. *Nat Rev Mol Cell Biol* 2019;**20**:353–367.

9. Deidda M, Piras C, Bassareo PP, Dessalvi CC, Mercuro G. Metabolomics, a promising approach to translational research in cardiology. *IJC Metab Endocr* 2015;**9**:31–38.

10. Johnson CH, Ivanisevic J, Siuzdak G. Metabolomics: beyond biomarkers and towards mechanisms. *Nat Rev Mol Cell Biol* 2016;**17**:451–459.

11. Liu X, Locasale JW. Metabolomics: a primer. *Trends Biochem Sci* 2017;**42**:274–284.

12. Burnum KE, Frappier SL, Caprioli RM. Matrix-assisted laser desorption/ionization imaging mass spectrometry for the investigation of proteins and peptides. *Annu Rev Anal Chem* 2008;**1**:689–705.

13. Chughtai S, Chughtai K, Cillero-Pastor B, Kiss A, Agrawal P, MacAleese L, et al. A multimodal mass spectrometry imaging approach for the study of musculoskeletal tissues. *Int J Mass Spectrom* 2012;**325-327**:150–160.

14. Tsai Y-H, Bhandari DR, Garrett TJ, Carter CS, Spengler B, Yost RA. Skeletal muscle fiber analysis by atmospheric pressure scanning microprobe matrix-assisted laser desorption/ionization mass spectrometric imaging at high mass and high spatial resolution. *Proteomics* 2016;**16**:1822–1824.

15. Tsai Y-H, Garrett TJ, Carter CS, Yost RA. Metabolomic analysis of oxidative and glycolytic skeletal muscles by matrix-assisted laser desorption/ionization mass spectrometric imaging (MALDI MSI). *J Am Soc Mass Spectrom* 2015;**26**:915–923.

16. Klein O, Strohschein K, Nebrich G, Oetjen J, Trede D, Thiele H, et al. MALDI imaging mass spectrometry: discrimination of pathophysiological regions in traumatized skeletal muscle by characteristic peptide signatures. *Proteomics* 2014;**14**:2249–2260.

17. Klein O, Strohschein K, Nebrich G, Fuchs M, Thiele H, Giavalisco P, et al. Unraveling local tissue changes within severely injured skeletal muscles in response to MSC-based intervention using MALDI Imaging mass spectrometry. *Sci Rep* 2018;**8**:12677.

18. Kunzke T, Buck A, Prade VM, Feuchtinger A, Prokopchuk O, Martignoni ME, et al. Derangements of amino acids in cachectic skeletal muscle are caused by mitochondrial dysfunction. *J Cachexia Sarcopenia Muscle* 2020;**11**:226–240.

19. Hu X, Charles JP, Akay T, Hutchinson JR, Blemker SS. Are mice good models for human neuromuscular disease? Comparing muscle excursions in walking between mice and humans. *Skeletal Muscle* 2017;**7**:26.

20. Henseler JF, Nagels J, Van Der Zwaal P, Nelissen RG. Teres major tendon transfer for patients with massive irreparable posterosuperior rotator cuff tears. *Bone Joint J* 2013;**95-B**:523–529.

21. Gomori G. A rapid one-step trichrome stain. *Am J Clin Pathol* 1950;**20**:661–664.

22. Buck A, Heijs B, Beine B, Schepers J, Cassese A, Heeren RM, et al. Round robin study of formalin-fixed paraffin-embedded tissues in mass spectrometry imaging. *Anal Bioanal Chem* 2018;**410**:5969–5980.

23. Lou S, Balluff B, Cleven AH, Bovée JV, McDonnell LA. An experimental guideline for the analysis of histologically heterogeneous tumors by MALDI-TOF mass spectrometry imaging. *Biochim Biophys Acta Proteins Proteomics* 2017;**1865**:957–966.

24. Wishart DS, Feunang YD, Marcu A, Guo AC, Liang K, Vázquez-Fresno R, et al. HMDB 4.0: the human metabolome database for 2018. *Nucleic Acids Res* 2018;**46**:D608–d617.

25. Kolk A, van der Zwaal P, Thomassen BJ, van de Kamp EW, Stijnen T, de Groot JH, et al. The presence of a rotator cuff tear interferes with age-dependent muscle atrophy of intact shoulder muscles. An MRI study with 3years' follow-up. *Hum Mov Sci* 2018;**62**:161–168.

26. Wegiel B, Nemeth Z, Correa-Costa M, Bulmer AC, Otterbein LE. Heme oxygenase-1: a metabolic nike. *Antioxid Redox Signal* 2014;**20**:1709–1722.

27. Hilber K, Galler S, Gohlsch B, Pette D. Kinetic properties of myosin heavy chain isoforms in single fibers from human skeletal muscle. *FEBS Lett* 1999;**455**:267–270.

28. Hanselmann C, Mauch C, Werner S. Haem oxygenase-1: a novel player in cutaneous wound repair and psoriasis? *Biochem J* 2001;**353**:459–466.

29. Takahashi T, Shimizu H, Morimatsu H, Maeshima K, Inoue K, Akagi R, et al. Heme oxygenase-1 is an essential cytoprotective component in oxidative tissue injury induced by hemorrhagic shock. *J Clin Biochem Nutr* 2009;**44**:28–40.

30. Grochot-Przeczek A, Lach R, Mis J, Skrzypek K, Gozdecka M, Sroczynska P, et al. Heme oxygenase-1 accelerates cutaneous wound healing in mice. *PLoS ONE* 2009;**4**:e5803.

31. Szentesi P, Csernoch L, Dux L, Keller-Pintér A. Changes in redox signaling in the skeletal muscle with aging. *Oxid Med Cell Longev* 2019;**2019**:4617801.

32. Park C-H, Ju TJ, Kim YW, Dan JM, Kim JY, Kim YD, et al. Hemin, heme oxygenase-1 inducer, attenuates immobilization-induced skeletal muscle atrophy in mice. *Life Sci* 2013;**92**:740–746.

33. Grabellus F, Schmid C, Levkau B, Breukelmann D, Halloran PF, August C, et al. Reduction of hypoxia-inducible heme oxygenase-1 in the myocardium after left ventricular mechanical support. *J Pathol* 2002;**197**:230–237.

34. Kozakowska M, Pietraszek-Gremplewicz K, Ciesla M, Seczynska M, Bronisz-Budzynska I, Podkalicka P, et al. Lack of heme oxygenase-1 induces inflammatory reaction and proliferation of muscle satellite cells after cardiotoxin-induced skeletal muscle injury. *Am J Pathol* 2018;**188**:491–506.

35. Pietraszek-Gremplewicz K, Kozakowska M, Bronisz-Budzynska I, Ciesla M, Mucha O, Podkalicka P, et al. Heme oxygenase-1 influences satellite cells and progression of

Duchenne muscular dystrophy in mice. *Antioxid Redox Signal* 2018;**29**:128–148.

36. Dutra FF, Bozza MT. Heme on innate immunity and inflammation. *Front Pharmacol* 2014;**5**:115.

37. Srivastava NK, Yadav R, Mukherjee S, Pal L, Sinha N. Abnormal lipid metabolism in skeletal muscle tissue of patients with muscular dystrophy: in vitro, high-resolution NMR spectroscopy based observation in early phase of the disease. *Magn Reson Imaging* 2017;**38**:163–173.

38. Lipina C, Hundal HS. Lipid modulation of skeletal muscle mass and function. *J Cachexia Sarcopenia Muscle* 2017;**8**: 190–201.

39. van der Veen JN, Kennelly JP, Wan S, Vance JE, Vance DE, Jacobs RL. The critical role of phosphatidylcholine and phosphatidylethanolamine metabolism in health and disease. *Biochim Biophys Acta Biomembr* 2017;**1859**:1558–1572.

40. Selathurai A, Kowalski GM, Mason SA, Callahan DL, Foletta VC, Della Gatta PA, et al. Phosphatidylserine decarboxylase is critical for the maintenance of skeletal muscle mitochondrial integrity and muscle mass. *Mol Metab* 2019;**27**:33–46.

41. Goto-Inoue N, Morisasa M, Machida K, Furuichi Y, Fujii NL, Miura S, et al. Characterization of myofiber-type-specific molecules using mass spectrometry imaging.

Rapid Commun Mass Spectrom 2019;**33**: 185–192.

42. Zemski Berry KA, Hankin JA, Barkley RM, Spraggins JM, Caprioli RM, Murphy RC. MALDI imaging of lipid biochemistry in tissues by mass spectrometry. *Chem Rev* 2011;**111**:6491–6512.

43. Ellis SR, Paine MR, Eijkel GB, Pauling JK, Husen P, Jervelund MW, et al. Automated, parallel mass spectrometry imaging and structural identification of lipids. *Nat Methods* 2018;**15**:515–518.

44. Buchberger AR, DeLaney K, Johnson J, Li L. Mass spectrometry imaging: a review of emerging advancements and future insights. *Anal Chem* 2018;**90**:240–265.